Available online at www.sciencedirect.com

ScienceDirect

Ceramics International 40 (2014) 2605–2611

CERAMICS INTERNATIONAL

www.elsevier.com/locate/ceramint

Microstructure development and phase evolution of alumina–mullite nanocomposite

A. Sedaghat[a], E. Taheri-Nassaj[a,*], G.D. Soraru[b], T. Ebadzadeh[c]

[a]Department of Materials Science and Engineering, Tarbiat Modares University, PO Box 14115-143, Tehran, Iran
[b]Department of Materials Engineering and Industrial Technology, University of Trento, Via Mesiano 77, 38050 Trento, Italy
[c]Materials & Energy Research Centre, PO Box 14155-4777, Tehran, Iran

Received 30 June 2013; received in revised form 23 September 2013; accepted 18 October 2013
Available online 25 October 2013

Abstract

In this work, the alumina–mullite composite was prepared using sol–gel derived alumina composite nanopowders. Results revealed the intragranular mullite was embedded in the alumina grain and the intergranular mullite was embedded on the grain boundary. Accordingly, the intragranular mullites (average grain size, 0.3 μm) were smaller than the intergranular mullites (average grain size, 0.5 μm). Moreover, the alumina grains (average grain size, 1.0 μm) are larger than the mullites. Meanwhile, the mullites showed positive results in the prevention of the alumina grains growth, known as the Zener law behavior, and the retardation of densification. The relative density of alumina–mullite that was sintered at 1650 °C for 2 h was obtained as 98.7%. After sintering at 1750 °C for 2 h, the mullite was decomposed.

Keywords: A. Sintering; B. Microstructure-final; D. Al_2O_3; D. Mullite

1. Introduction

Alumina–mullite ceramics may have a high potential for armour and wear resistance applications [1,2]. The important applications of alumina–mullite composite are components and structures for gas turbine engines, burner tubes and heat shields for re-entry space vehicles [3]. Mullite in the alumina matrix reduces the Young's modulus and thermal expansion coefficient of the composite, leading to a better thermal shock resistance [4–6]. Meanwhile, mullite has low toughness and hardness [7]. Small mullite additions (5–15 vol%) allow desirable values of hardness and toughness of alumina to be maintained while reducing the Young's modulus below that of alumina, so that it is expected that the thermal shock behaviour will be improved [8].

A number of recent works have involved the addition of impurities in order to achieve better densification behaviour and, as a consequence, higher densities and better microstructures and mechanical properties [9,10]. Schehl et al. [11] presented a modified processing route which consists in the doping of a commercial high-purity alumina powder so that its microstructure is modified with such nanoparticles as zirconia and mullite, formed at the sintering stage. As a result, the grain boundaries of the high-purity alumina powder are modified by segregation of the secondary phases or by the formation of well-distributed zirconia and mullite nanoparticles. Thus it should be possible to tailor microstructures by means of secondary phases by referring to the corresponding phase equilibrium diagrams.

Very high homogeneous multicomponent ceramics and composite ceramics can be obtained via sol–gel method, since the synthesis temperature of this method is low [12].

In this work, alumina–mullite composites (5–15 vol%) were prepared using sol–gel derived alumina composite nanopowders, with the ultimate aim to investigate the positioning of mullite and its effect on the microstructure of the alumina–mullite composite. Meanwhile, the phase evolution of this composite was studied.

2. Experimental

The flowchart of the procedure is shown in Fig. 1. Homogeneous distribution of mullite in the matrix of alumina can be

*Corresponding author. Tel.: +98 21 82883306; fax: +98 21 88005040.
E-mail address: taheri@modares.ac.ir (E. Taheri-Nassaj).

0272-8842/$ - see front matter © 2013 Elsevier Ltd and Techna Group S.r.l. All rights reserved.
http://dx.doi.org/10.1016/j.ceramint.2013.10.071

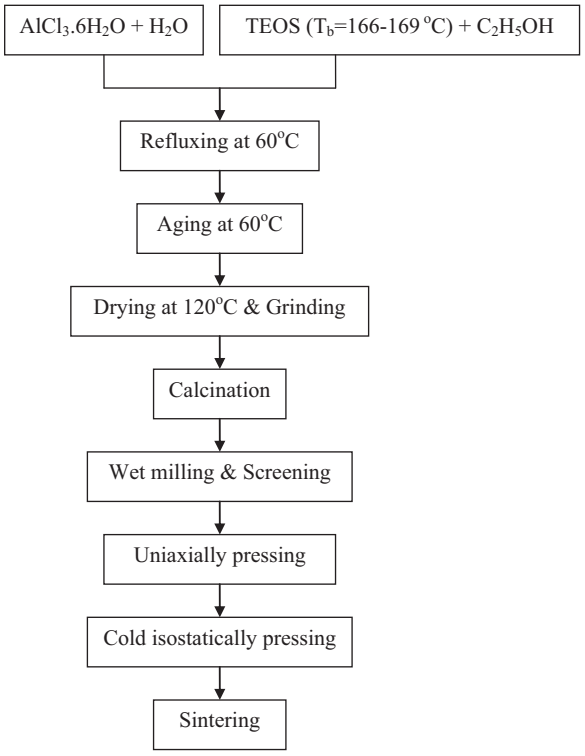

Fig. 1. The flow chart of the processing of alumina–mullite nanocomposite.

Table 1
Properties of the alumina—15 vol% mullite precursor calcined at 900 °C for 2 h.

BET surface area [m^2/g]	105.4 ± 0.4
Apparent density [g/cm^3]	3.646 ± 0.007
Mean particle size [nm]	15
Surface area of pores [m^2/g]	106
Total pore volume [cm^3/g]	0.50
Average pore diameter (4V/A by BET) [nm]	19.0

obtained through sol–gel method. So the alumina composite nanopowders (Table 1) were synthesized by sol–gel method. Aluminum chloride hexahydrate (Merck 101084) was dissolved in distilled water and tetraethyl orthosilicate (Sigma-Aldrich 131903) was dissolved in absolute ethanol. Based on the stoichiometric ratio ($3Al_2O_3$ $2SiO_2$) and the desired volume percentage (0, 5, 10, 15 vol%) of mullite, the aqueous solution of salt with the required amount of the alcoholic solution of tetraethyl orthosilicate (TEOS) was refluxed at 60 °C for 24 h. After condensation, the gel was dried at 120 °C for 24 h and ground in an agate mortar. The precursors of the alumina and the alumina–mullite composites were calcined at 900 °C for 2 h and subsequently attrition-milled with high purity alumina balls and absolute ethanol for 1 h. After drying, the powders were sieved using an 80 μm mesh.

Fig. 2 presents isotherm patterns of nitrogen adsorption–desorption (a) and pore distribution of alumina-15 vol% mullite precursor calcined at 900 °C for 2 h (b). It can be seen that the powder exhibits the Type IIb group with the presence of mesopores. Shape of the curve and the hysteresis loop (H3-type) can justify the presence of aggregates containing platy particles (alumina shows this typical behavior) with the

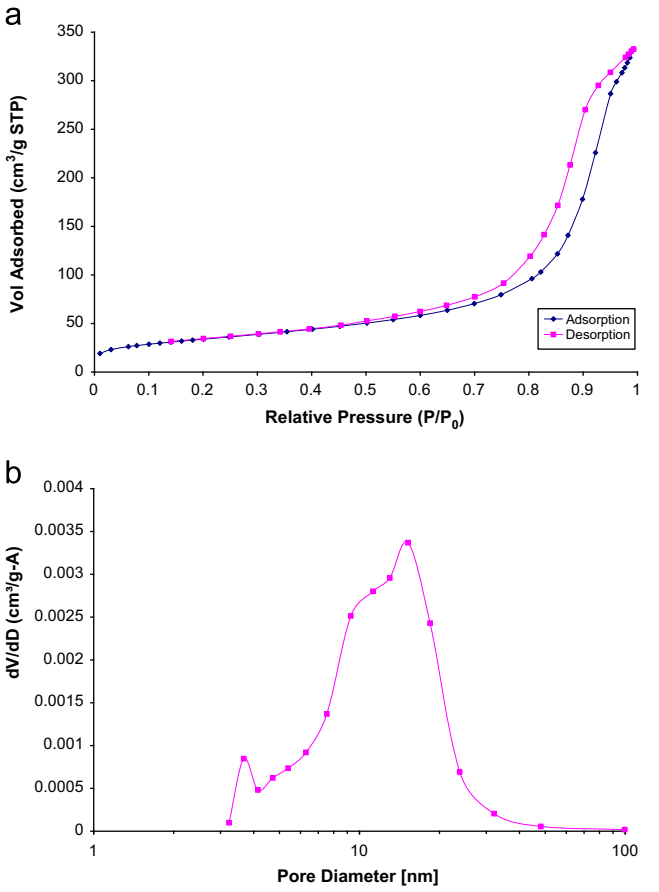

Fig. 2. (a) Nitrogen adsorption–desorption isotherm and (b) pore distribution of the alumina–mullite 15 vol% precursor calcined at 900 °C for 2 h.

presence of non-rigid slit-shaped pores which were formed by the aggregates. These platy particles can be observed in the TEM micrograph (Fig. 3(a) and (b)) presents the smaller particles.

The powders were uniaxially pressed under 38 MPa. Then they were cold isostatically pressed (CIP) at 380 MPa for achieving greater uniformity of compaction, and finally sintered in air at 1650 °C for 2 h. Moreover, the alumina-15 vol% mullite specimens were sintered at 1300, 1500, 1650 and 1750 °C for 2 h to investigate their microstructure development.

X-ray diffraction (XRD) was carried out for phase characterization of the alumina and the alumina–mullite composites (5, 10 and 15 vol%) sintered at 1650 °C for 2 h. The phase evolution of the alumina-15 vol% mullite, thermally treated at different temperatures (400–1750 °C), was studied by XRD. The XRD patterns were recorded in the range of $10 < 2\theta < 80$ using Philips X-pert model with Cu $K\alpha$.

The microstructure of the sintered bodies was studied by a XL 30, Field Emission Environmental Scanning Electron Microscope (FEI-Philips) equipped with a Link Energy Dispersive X-ray system. The specimens for SEM were polished to 1 μm surface finish using diamond spray. Thereafter, they were thermally etched for 1 h at 100 °C below the sintering temperature. The average grain size was defined as the average apparent

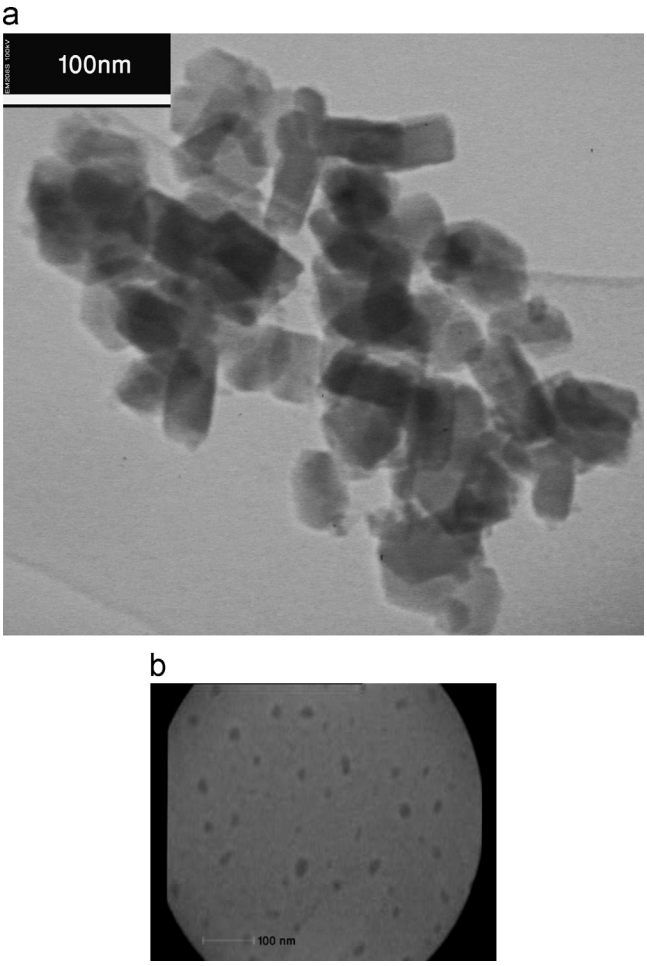

Fig. 3. The TEM micrograph (bright field) of alumina-15 vol% mullite precursor calcined at 900 °C for 2 h (average particle size, 31 nm).

diameter of the grains determined directly by using image analysis software. Moreover, the average length and width of the grains were measured on the elongated grains.

Powder morphology and microstructure characterization of the sintered specimens was performed by transmission electron microscopy (TEM) employing a Philips CM12 instrument, while the instrument was operated at 120 kV. The bulk specimens were prepared following the standard grinding and ion-polishing procedures.

The Archimedes method [13] was used in this work to measure the density of the samples sintered by using distilled water as an immersion medium and determining three mass values (dry, suspended and saturated masses). Moreover, the relative density was calculated by dividing the bulk density to the theoretical density of the specimen.

3. Results and discussion

As shown in Fig. 4, the alumina and the alumina–mullite composites were prepared with the desired amounts of mullite (5, 10 and 15 vol%) after sintering at 1650 °C for 2 h. This assumption was supported by a modified Rietveld method [14]. The microstructures of these samples are shown in Fig. 5

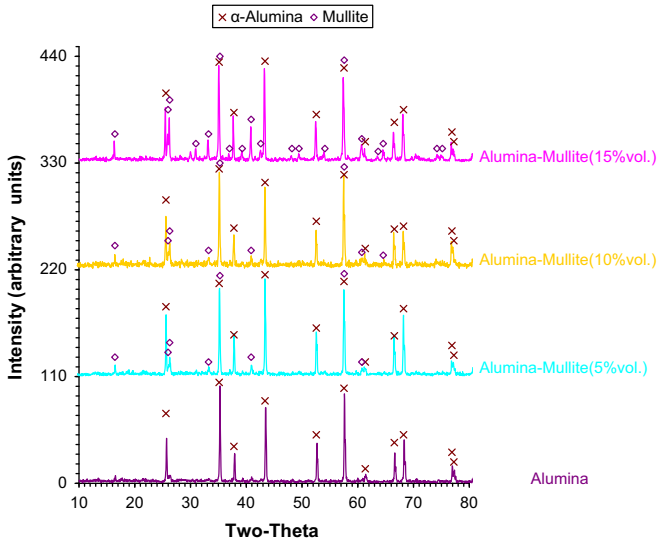

Fig. 4. The XRD patterns of alumina–mullite composites sintered at 1650 °C for 2 h.

(a–d). Fig. 5 depicts a reducing of the grain size of both alumina and mullite by increasing mullite content. The average grain size of alumina-0, 5, 10 and 15 vol% mullite (Fig. 5) are 1.6, 1.3, 0.9 and 0.8 μm, respectively. Accordingly, the addition of tetraethyl orthosilicate to the alumina composite precursor has positive results in the prevention of the alumina grain growth.

Grain growth can be inhibited through grain-boundary pinning by secondary particles (zener pinning) [15]. Most of the intentionally added dopants present a low limit of solubility in alumina and are thus segregated to grain boundaries. When pure alumina is doped over the solubility limit with large size cations like Y^{3+} and Zr^{4+}, a pinning effect takes place at grain boundaries due to the formation of other phases such as zirconia, YAP and YAG [11]. The pinning process blocks grain accommodation during the sintering. In this work, the mullite particles inhibited the grain growth. So the reducing of the grain size is observed by increasing mullite content (Fig. 5).

The microstructure of the alumina-10 vol% mullite composite in BSE (Backscattered electrons) mode is shown in Fig. 6. The EDAX analyses of light areas (Point A) reveal the aluminum (Al) and oxygen (O) peaks and the EDAX analyses of dark areas (Point M) depict the Al, O and Si peaks. On the other hand, the XRD patterns of these samples (Fig. 4) reveal both alumina and mullite. So the light and dark areas are alumina and mullite, respectively. Fig. 5 depicts that the intragranular mullite was embedded in the alumina grain and the intergranular mullite was embedded on the grain boundary.

Schehl et al. [11] prepared alumina composites from powder-alkoxide mixtures (alpha alumina powder with $d_{50}=0.46$ μm and tetraethyl orthosilicate). They presented a microstructure of the alumina composite, after sintering at 1600 °C for 2 h, with a mean grain size of 1.88 μm and the mullite phase (dark areas) located at the triple points, not inside the alumina grains. Fig. 6 shows the TEM micrograph (bright

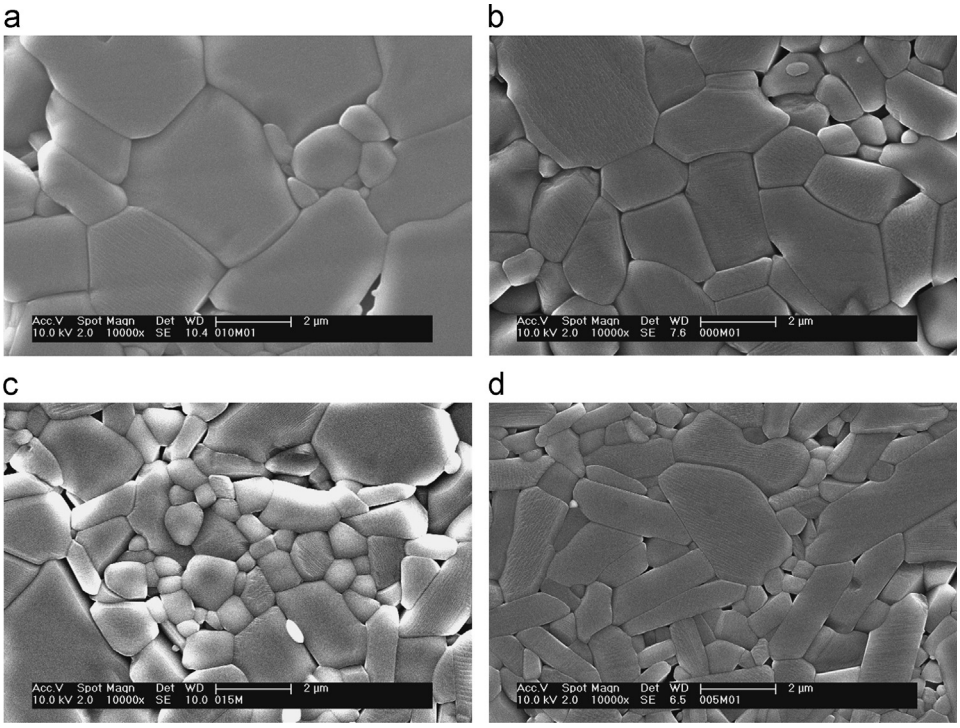

Fig. 5. The FESEM micrographs (SE Mode) of alumina–mullite composites sintered at 1650 °C for 2 h: (a) 0 vol% mullite (average grain size, 1.6 μm). (b) 5 vol% mullite (average grain size, 1.3 μm). (c) 10 vol% mullite (average grain size, 0.9 μm). (d) 15 vol% mullite (average grain size, 0.8 μm).

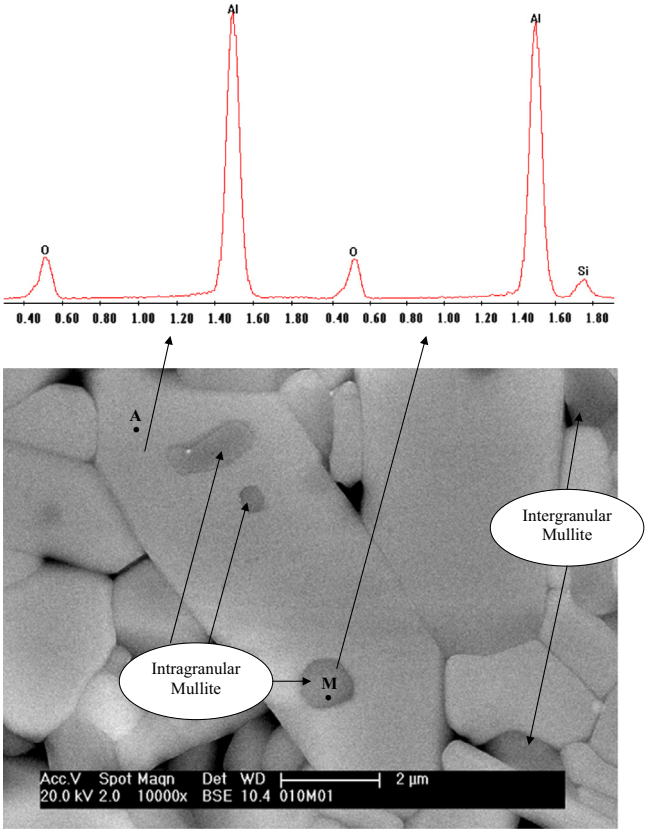

Fig. 6. The FESEM micrograph (BSE Mode) of alumina-10 vol% mullite composite sintered at 1650 °C for 2 h and the EDAX analysis of points A and M (A: alumina, M: mullit).

field) of the sintered alumina-5 vol% mullite composite at 1650 °C for 2 h and the EDAX analysis of point M. Also a spherical mullite particle with 190 nm diameter was observed inside one of the alumina grains. The size of the intragranular mullite (average particle size, 0.3 μm) is lower than that of the intergranular mullite (average grain size, 0.5 μm) and the intergranular mullite grains are smaller than the alumina grains (average grain size, 1.0 μm).

After sintering at 1650 °C for 2 h, the relative density of the alumina was obtained as 99.3 ± 0.3%T.D.,[1] which was reduced to 98.7 ± 0.3%T.D. in the presence of mullite. It was shown that the relative density of alumina (99.3%) was more than the alumina–mullite nanocomposites (98.8%) but the variation of density of composites is inside the experimental error. On the other hand, the mullite retards the densification.

In another work [16], an alumina mat was prepared by sol–gel technique using aluminum chloride hexahydrate with different amounts of colloidal silica (0, 2, 4, 6 and 8 wt% SiO_2). The transitional alumina was transformed into alpha alumina at 1000 °C, and by increasing the silica content, this phase transformation was retarded to 1200 °C. Fig. 7 presents the XRD patterns of the alumina-15 vol% mullite that was thermally treated at different temperatures (400–1750 °C). Moreover, it reveals that the transitional alumina [17] was transformed into alpha alumina [18] at 1000 °C and the source of SiO_2 was tetraethyl orthosilicate, not colloidal silica. So it is

[1]The individual data points were 99.03, 99.26, 99.30, 99.41, 99.73.

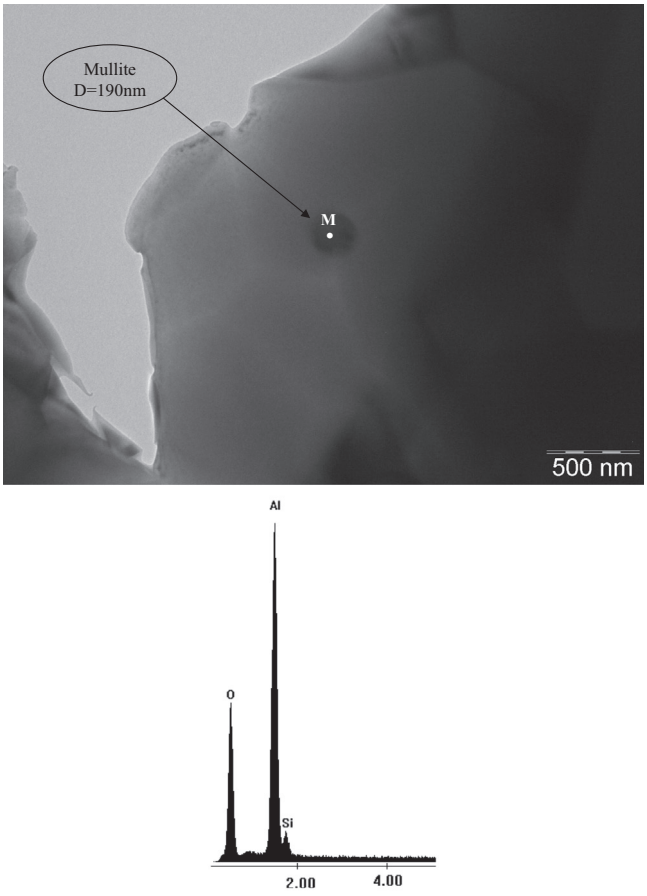

Fig. 7. The TEM micrograph (bright field) of alumina-5 vol% mullite composite sintered at 1650 °C for 2 h and the EDAX analysis of point M.

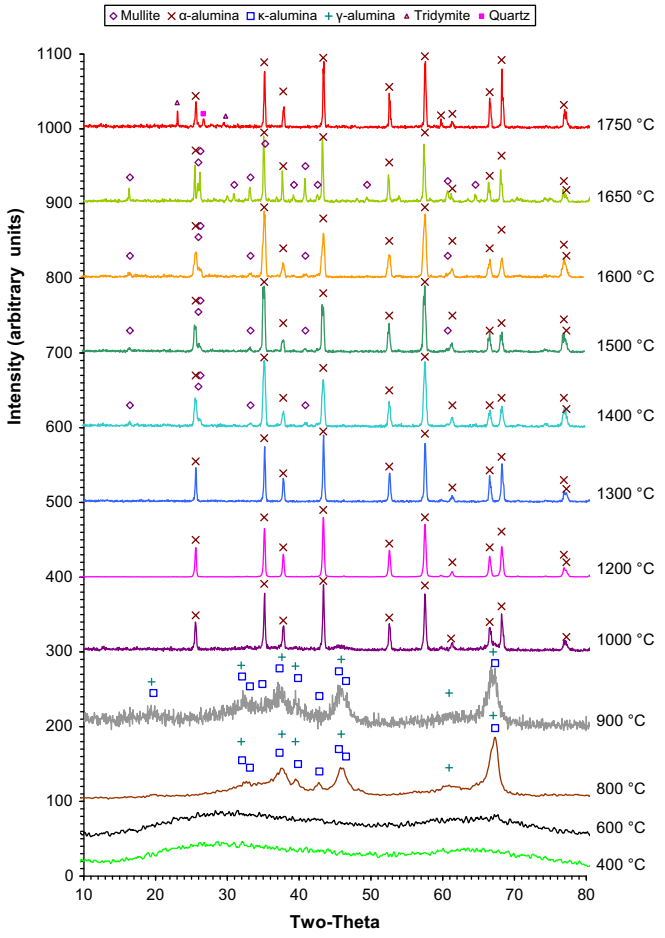

Fig. 8. The XRD patterns of alumina-15 vol% mullite precursor calcined at different temperatures (400–1750 °C).

supposed that the phase transformation was not retarded due to the dissolution of tetraethyl orthosilicate. The mullite peaks [19] were detected by increasing the sintering temperature.

The XRD pattern of the alumina-15 vol% mullite that was thermally treated at 1750 °C for 2 h (Fig. 8) depicts alpha alumina peaks [18] and some peaks of quartz [20] and tridymite [21]. Decomposition of mullite has been reported at high temperature in reducing atmospheres [22]. For example, mullite specimen surfaces had heat-treated in helium between 1650 °C and 1800 °C, degrade with the formation of alpha alumina and volatile silicon species, so that the recession progresses from the surface towards the bulk of specimens. So it can be supposed that in the samples of this work, the mullite was decomposed at 1750 °C by the following reactions [22]:

$$3Al_2O_3 \cdot 2SiO_2(s) \rightarrow 3Al_2O_3(s) + 2SiO(g) + O_2(g) \quad (1)$$

$$2SiO(g) + O_2(g) \rightarrow 2SiO_2(g) \quad (2)$$

Net reaction:

$$3Al_2O_3 \cdot 2SiO_2\ (\text{mullite}) \rightarrow 3Al_2O_3\ (\text{alpha alumina}) + 2SiO_2\ (g) \quad (3)$$

s = solid, g = gaseous

The microstructure of alumina-15 vol% mullite composite that was sintered at 1750 °C for 2 h (Fig. 9) reveals a grain growth. Meanwhile, the average grain size was calculated as 2.2 μm at 1750 °C. The micrograph was taken in BSE mode to investigate the phase evolution. There are dark and light areas. The EDAX analyses (Fig. 9(b and c)) and XRD pattern (Fig. 8) of these areas revealed that the silica particles (dark areas) are embedded in the alumina grains (light areas) at 1750 °C. Moreover, some pores are observed due to sintering or mullite decomposition. In addition, the TEM micrograph (bright field) and EDAX analysis of alumina-15 vol% mullite composite that has been sintered at 1750 °C for 2 h are observed in Fig. 10. The presence of silica in the fracture edge is revealed by the EDAX analysis of point S (Fig. 10) and its XRD pattern (Fig. 8). There is also another pore with 300 nm diameter due to sintering or mullite decomposition.

Fig. 10 shows the densification of alumina-15 vol% mullite after being sintered at different temperatures (1300–1750 °C) for 2 h. After sintering, the relative density increased by increasing of the temperature (Fig. 11). At 1500, 1650 and 1750 °C, the relative densities were calculated as 67.2 ± 0.3, 98.7 ± 0.3 and 98.6 ± 0.4, respectively. At 1500 °C, the densification was not completed and at 1750 °C, the mullite was decomposed according to Fig. 11. So it was preferred to sinter at 1650 °C.

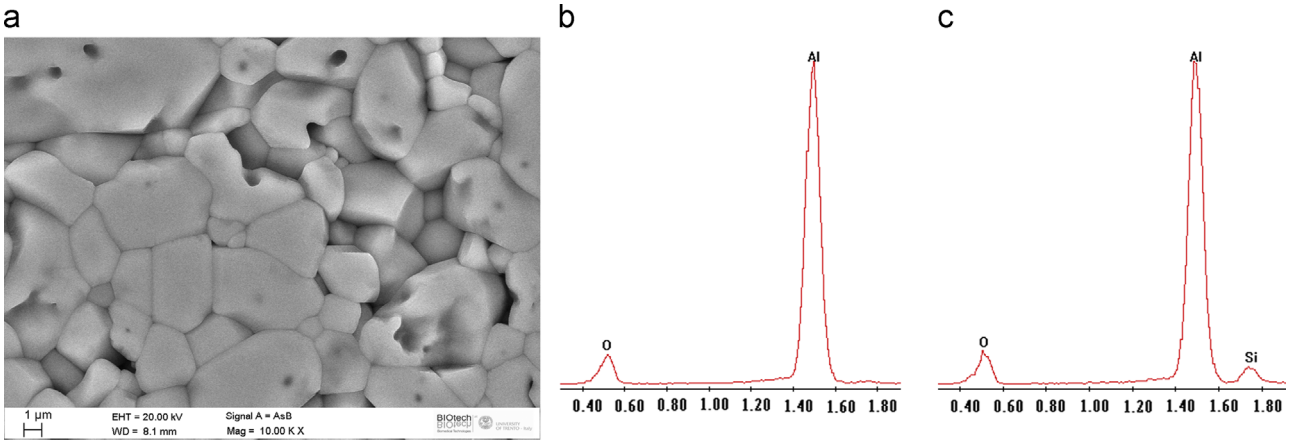

Fig. 9. The FE-SEM micrograph (BSE Mode) of alumina-15 vol% mullite composite sintered at 1750 °C for 2 h (a) with the EDAX analysis of light (b) and dark (c) areas (99.3% T.D., average grain size, 2.2 μm).

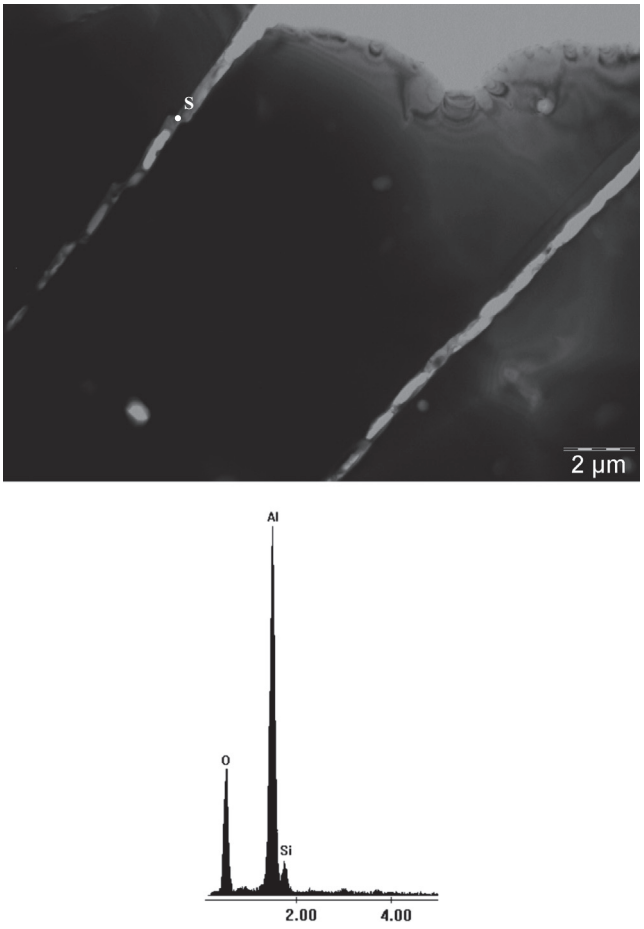

Fig. 10. The TEM micrograph (bright field) of alumina-15 vol% mullite composite sintered at 1750 °C for 2 h and EDAX analysis of point S.

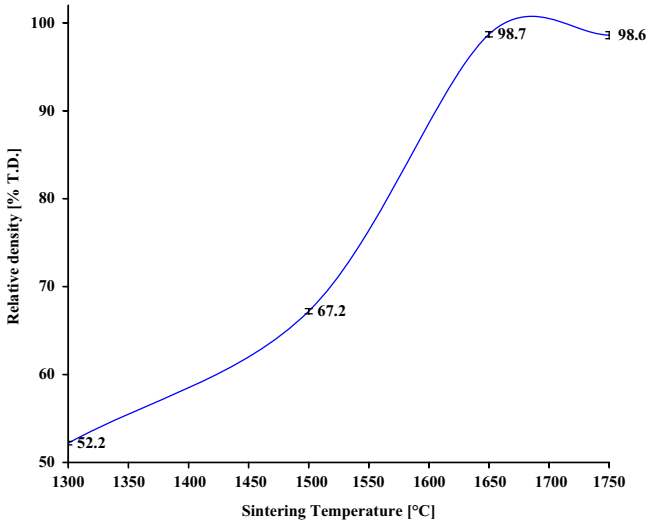

Fig. 11. The relative densities of alumina-15 vol% mullite after being sintered at 1300–1750 °C for 2 h.

4. Conclusions

In this work, the alumina composite nanopowders, synthesized via sol–gel method using aluminum chloride hexahydrate and tetraethyl orthosilicate, were used to prepare the alumina–mullite composite by pressing, CIP and sintering. The findings are summarized as follows:

1. The intragranular mullite was embedded in the alumina grain and the intergranular mullite was embedded on the grain boundary.
2. The grain size of the intragranular mullite (average grain size, 0.3 μm) is lower than that of the intergranular mullite (average grain size, 0.5 μm). Moreover, that of the intergranular mullite is lower than that of the alumina (average grain size, 1.0 μm).
3. The mullite showed positive results in the prevention of the alumina grain growth and also in the retardation of densification.
4. The relative density of alumina–mullite composite sintered at 1650 °C for 2 h, was calculated as 98.7%.
5. After sintering at 1750 °C for 2 h, the mullite was decomposed and some pores were observed due to sintering or mullite decomposition.

Acknowledgements

The authors wish to thank Francesco Tessarolo (section of Electron Microscopy, Department of Medicine Laboratory-APSS Trento) for FE-SEM microstructural characterizations.

References

[1] D.W. Richerson, Modern Ceramic Engineering, Marcel Dekker New York, 1992, p. 808–823.
[2] E. Medvedovski, Alumina–mullite ceramics for structural applications, Ceram. Int. 32 (2006) 369–375.
[3] H. Schneider, J. Schreuer, B. Hildmanu, Structure and properties of mullite—a review, J. Eur. Ceram. Soc. 28 (2008) 329.
[4] S. Mezquita, R. Uribe, R. Moreno, C. Baudín, Influence of mullite additions on thermal shock resistance of dense alumina materials Part 2: Thermal properties and thermal shock behavior, Br. Ceram. Trans. 100 (6) (2001) 246–250.
[5] C. Aksel, The effect of mullite on the mechanical properties and thermal shock behaviour of alumina–mullite refractory materials, Ceram. Int. 29 (2003) 183–188.
[6] F.C. Zhang, H.H. Luo, S.G. Roberts, Mechanical properties and microstructure of Al_2O_3/mullite composite, J. Mater. Sci. 42 (2007) 6798–6802.
[7] C. Aksel, The role of fine alumina and mullite particles on the thermomechanical behaviour of alumina–mullite refractory materials, Mater. Lett. 57 (2002) 708–714.
[8] R. Moreno, S. Mezquita, C. Baudín, Influence of mullite additions on thermal shock resistance of dense alumina materials Part 1: Processing studies, Br. Ceram. Trans. 100 (6) (2001) 241–245.
[9] A.M. Thompson, K.K. Soni, H.M. Chan, M.P. Harmer, D.B. Williams, J.M. Chabala, R. Levi-Scotti, Dopant distributions in rare-earth-doped alumina, J. Am. Ceram. Soc. 80 (2) (1997) 373–376.
[10] J. Fang, A.M. Thompson, M.P. Harmer, H.M. Chan, Effect of yttrium and lanthanum on the final-stage sintering behavior of ultrahigh-purity alumina, J. Am. Ceram. Soc. 80 (8) (1997) 2005–2012.
[11] M. Schehl, L.A. Díaz, R. Torrecilla, Alumina nanocomposites from powder–alkoxide mixtures, Acta Mater. 50 (2002) 1125–1139.
[12] C.W. Won, B. Siffert, Preparation by sol–gel method of SiO_2 and mullite ($3Al_20_3$ $2SiO_2$) powders and study of their surface characteristics by inverse gas chromatography and zetametry, Colloid Surf. A 13 (1998) 161–172.
[13] 'Standard Test Method for Water Absorption, Bulk Density, Apparent Porosity, and Apparent Specific Gravity of Fired Whiteware Products', ASTM Designation: C 373-88, ASTM Standards, Vol. 15.02, 2005.
[14] L. Lutterotti, R. Ceccato, R. Dal Maschio, E. Pagani, Quantitative analysis of silicate glass in ceramic materials by the Rietveld method, Mater. Sci. Forum. 87 (1998) 278–281.
[15] M.N. Rahaman, Ceramic Processing and Sintering, Marcel Dekker, New York, 2003, p. 574–580.
[16] A. Sedaghat, E. Taheri-Nassaj, R. Naghizadeh, An alumina mat with a nano microstructure prepared by centrifugal spinning method, J. Non-Cryst. Solids 352 (2006) 2818–2828.
[17] Powder Diffraction File, Card No. 10-0425, JCPDS.
[18] Powder Diffraction File, Card No. 10-0173, JCPDS.
[19] Powder Diffraction File, Card No. 15-0776, JCPDS.
[20] Powder Diffraction File, Card No. 01-087-2096, JCPDS.
[21] Powder Diffraction File, Card No. 01-085-0419, JCPDS.
[22] H. Schneider, S. Komarneni, Mullite, WILEY-VCH Verlag GmbH and Co. KGaA, Weinheim, 2005, p. 236–237.